RSC Advances

PAPER

View Article Online
View Journal | View Issue

Cite this: *RSC Adv.*, 2015, **5**, 85453

Ammonia selective catalytic reduction of NO over Ce–Fe/Cu–SSZ-13 catalysts

Xiaojiao Liu,[abc] Yonghong Li*[abc] and Ranran Zhang[abc]

Received 10th August 2015
Accepted 24th September 2015

DOI: 10.1039/c5ra16072c

www.rsc.org/advances

A series of CHA-type trimetallic composite zeolites of Ce_x–Fe_y/Cu–SSZ-13 catalysts were prepared using Cu–SSZ-13, synthesized in a one-pot procedure, and subsequent ion-exchange with Fe^{3+} and Ce^{3+}. The catalysts were characterized including TEM, XRD, XPS, SEM and BET. Their catalytic performances for selective catalytic reduction of NO with NH_3 were investigated. The results of XRD revealed that the crystal structure of zeolite Ce–Fe/Cu–SSZ-13 is the same as Cu–SSZ-13. It is known from the results of BET and catalytic performance tests that larger specific surface areas and smaller pore size favor a catalytic reaction. Among the prepared Ce_x–Fe_y/Cu–SSZ-13 catalysts, $Ce_{0.017}$–$Fe_{0.017}$/Cu–SSZ-13 displayed the best SCR performance. The NO conversion was more than 90% between 200 and 500 °C. N_2 selectivity was above 98% within the wider temperature range of 150–550 °C. In addition, the catalyst demonstrated sulfur–water tolerance and effective resistance against high space velocity. The phenomena suggest that synergistic effects of Cu, Fe and Ce species improve the SCR performances and make the Ce–Fe/Cu–SSZ-13 catalyst a promising candidate for NH_3–SCR technology.

Introduction

Nitrogen oxides emitted by diesel engines are a major kind of air pollutant that are responsible for acid rain, photochemical smog and ozone depletion. With legislation of NO_x emissions becoming more and more stringent, it is urgent to find an effective way to remove such pollutants from exhaust fumes. Nowadays, one of the most promising technologies to eliminate NO_x pollution is selective catalytic reduction (SCR) of NO_x with ammonia.[1] Recently, Cu/zeolite catalysts with chabazite (CHA) crystal structure, such as Cu–SSZ-13, has received much attention.[2,3] Cu–SSZ-13 prepared by an ion-exchange method is much more active, selective and hydrothermally stable than Cu-beta and Cu–ZSM-5.[4,5] However, the template *N*,*N*,*N*-trimethyl-1-adamantammonium hydroxide (TMAdaOH) used in the synthesis of SSZ-13 by Zones[6,7] is rather expensive. Therefore, it is desirable to find a substitute for the template TMAdaOH. Nuria *et al.*[8] suggested that low-cost methodologies to synthesize Cu-containing CHA catalysts using tetraethylammonium (TEA) as organic structure directing agent (OSDA) could be competitive and attractive for NH_3–SCR of NO_x. In addition, an economical method for SSZ-13 preparation with inexpensive choline chloride as template has been attempted by Chen *et al.*[9] and the as-synthesized SSZ-13 zeolite, ion-exchanged by copper nitrate solution, exhibited excellent SCR performance. Furthermore, Ren *et al.*[10] first used low-cost copper–amine complex as the template for the one-pot synthesis of Cu–SSZ-13 zeolite. Later, Xie *et al.*[11] further improved the synthesis of the Cu–SSZ-13 catalyst and indicated that the one-pot synthesized Cu–SSZ-13 catalyst was a promising candidate for NO_x elimination from diesel engine exhaust.

At present, more and more researchers are interested in heterobimetallic zeolites because of the complementary advantages and synergistic effects. In order to further improve the activity of the one-pot synthesized Cu–SSZ-13 catalyst, Zhang *et al.*[12] prepared Fe_x/Cu–SSZ-13 catalysts by incorporating Fe^{3+} into Cu–SSZ-13 and the catalysts exhibited high NH_3–SCR activity, excellent N_2 selectivity, robust hydrothermal stability and good tolerance to high space velocity. Ceria has been widely used as an additive for various catalysts because of its excellent oxygen storage capacity and high redox ability *via* Ce^{4+} to Ce^{3+} transition.[13–15] Herein, we attempt to modify the Cu/SSZ-13 catalyst with both iron and cerium to develop a more efficient NH_3–SCR catalyst for potential application in diesel engine exhaust treatment. In this study, the effects of Fe/Ce ratio, gas hourly space velocity (GHSV) and the concentration of O_2 on the activities for NO reduction are systematically investigated. In addition, the tolerance of the catalyst to H_2O, SO_2 and CO_2 was studied. The catalysts were further characterized through X-ray powder diffraction (XRD), transmission electron microscope (TEM), N_2 adsorption–desorption (BET), scanning electron microscope (SEM) and X-ray photoelectron spectra (XPS).

[a]*Key Lab for Green Chemical Technology of Ministry of Education, School of Chemical Engineering and Technology, Tianjin University, Weijin Road 92, Tianjin 300072, China. E-mail: yhli@tju.edu.cn; Fax: +86 022 27404705; Tel: +86 022 27404701 extn 8858*

[b]*National Engineering Research Center for Distillation Technology, Tianjin 300072, China*

[c]*Collaborative Innovation Center of Chemical Science and Engineering (Tianjin), Tianjin 300072, China*

Experimental

Preparation of Ce–Fe/Cu–SSZ-13 catalysts

Cu–SSZ-13 was synthesized by a one-pot hydrothermal synthesis method as reported by Zhang.[12] Ce_x–Fe_y/Cu–SSZ-13 catalysts were prepared by subsequent aqueous ion-exchange method. The specific steps are as follows: a certain amount of Cu–SSZ-13 was slowly added into $Fe(NO_3)_3 \cdot 9H_2O$ solution, with constant stirring at 80 °C for 8 h. The formed precipitate was washed with deionized water followed by drying at 110 °C and then exchanged with $Ce(NO_3)_3 \cdot 6H_2O$ solution. Finally, the sample was calcined at 550 °C for 5 h. We chose the optimum concentration of $Fe(NO_3)_3 \cdot 9H_2O$ solution at 0.017 mol L^{-1} according to a report by Zhang[12] and obtained a series of Ce_x–Fe_y/Cu–SSZ-13 catalysts through changing the concentration of $Ce(NO_3)_3 \cdot 6H_2O$. The x and y represent concentration (unit: mol L^{-1}) of the $Ce(NO_3)_3 \cdot 6H_2O$ solution and $Fe(NO_3)_3 \cdot 9H_2O$ solutions, respectively. The metal weight percentages in the catalysts were measured by ICP analysis. All chemicals used were purchased from Tianjin Huadong Reagent Factory.

Activity measurements

The "standard NH_3–SCR" experiments were performed in a fixed bed reactor (inner diameter 5 mm). The simulated exhaust gases were composed of 500 ppm NO, 500 ppm NH_3, 5 vol% O_2, 5 vol% H_2O (when used), 100 ppm SO_2 (when used), 5 vol% CO_2 (when used) and balance N_2. The total flow rate was 300 mL min^{-1} and thus a GHSV from 60 000 h^{-1} to 300 000 h^{-1} was obtained by changing the volume of the catalyst. The water vapor was injected by a pump (LSP01-1A, Longer Pump Inc.) and an evaporator. A K-type thermocouple was inserted into the center of catalyst bed from the bottom of the reactor and it was connected to a temperature programmed control instrument to monitor the reaction temperature. The concentration of NH_3, NO, NO_2 and N_2O were measured by a Thermo Nicolet IS10 Fourier-transform infrared (FTIR) spectrometer. NO conversion and N_2 selectivity of NH_3–SCR reaction were defined as:

$$\text{NO conversion} = (1 - [\text{NO}]_{\text{outlet}}/[\text{NO}]_{\text{inlet}}) \times 100\%;$$

$$\text{N}_2\text{ selectivity} = (([\text{NH}_3]_{\text{inlet}} - [\text{NO}]_{\text{outlet}} - [\text{NO}_2]_{\text{outlet}} - 2[\text{N}_2\text{O}]_{\text{outlet}} - [\text{NH}_3]_{\text{outlet}})/([\text{NH}_3]_{\text{inlet}} - [\text{NH}_3]_{\text{outlet}})) \times 100\%$$

Characterizations

Powder XRD patterns were obtained by a D8-Focus X-ray diffractometer with Cu Kα radiation (40 kV, 40 mA, λ = 0.15418 nm). Diffractometer data were obtained with a step size of 5° for 2θ values from 5° to 40°.

Nitrogen adsorption/desorption isotherms was measured at 77 K with a Micromeritics Tristar-3000 analyzer. Each sample was degassed for 1 h at 90 °C and another 3 h at 300 °C under N_2 atmosphere before the measurement. The specific surface area was calculated using standard BET method at a relative pressure (P/P_0) range of 0.05–0.35 and the V–t plot method was utilized to calculate the pore volume.

The morphology of the catalysts was observed by a field emission scanning electron microscope (FESEM, Nanosem 430). X-ray photoelectron spectroscopy (XPS) analysis was conducted with a PHI-1600 instrument using Mg Kα radiation (1253.6 eV) as X-ray source. TEM observations were carried out using a Tecnai G^2 F-20 transmission electron microscope with a field-emission gun operating at 200 kV.

Results and discussion

The influence of ion exchange level on NH_3–SCR activity

The catalytic activity of Ce_x–Fe_y/Cu–SSZ-13 (x = 0–0.15, y = 0.017) was studied from 150 °C to 550 °C under 150 000 h^{-1}. Fig. 1(a) shows NO conversion *vs.* temperature. The NO conversion over Ce_x–Fe_y/Cu–SSZ-13 (x = 0.006–0.15, y = 0.017) increased rapidly below 200 °C and reached above 90% in the temperature range of 200 °C to 500 °C. Especially within the temperature range of 150 to 225 °C, NO conversion increased significantly with x increasing from 0 to 0.017. For example, the NO conversion over Ce_0–$Fe_{0.017}$/Cu–SSZ-13 and $Ce_{0.017}$–$Fe_{0.017}$/Cu–SSZ-13 at 175 °C are 76.8% and 86.2%, respectively. However, there was only a little increase of NO conversion with x increasing from 0 to 0.017 within the temperature range of 250 to 550 °C. In addition, NO conversion decreased with x increasing from 0.017 to 0.15 between 150 °C and 550 °C due to the blocking of the "channel" of zeolites.[12] Clearly, $Ce_{0.017}$–$Fe_{0.017}$/Cu–SSZ-13 showed the best catalytic activity in a wider operation temperature window from 150 to 550 °C. As presented in Fig. 1(b), there was almost no NO_2 in the outlet gases and the concentration of N_2O was less than 6 ppm. Obviously, the concentration of N_2O reached a maximum value at 250 °C, which corresponds to the lowest N_2 selectivity. Fig. 1(b) also showed that N_2 selectivity over $Ce_{0.017}$–$Fe_{0.017}$/Cu–SSZ-13 catalyst was above 98% in the temperature between 150 °C and 550 °C, which made Ce–Fe/Cu–SSZ-13 catalyst as a promising candidate for NH_3–SCR technology.

Effects of GHSV on NH_3–SCR activity

The NH_3–SCR catalyst in diesel vehicles usually undergoes different GHSV in the practical application. Fig. 2 shows NO conversion over $Ce_{0.017}$–$Fe_{0.017}$/Cu–SSZ-13 under different GHSV. It was clear that with the increase of GHSV from 60 000 h^{-1} to 300 000 h^{-1}, NO conversion decreased significantly at low temperature, below 200 °C, yet there was only a little effect on the higher temperature (225–350 °C) SCR activity. Especially within the temperature range of 400 °C to 550 °C, there was almost no effect on NO conversion. Remarkably, the catalyst showed high NO conversion exceeding 90% during the temperature range of 225 to 500 °C under a rather high GHSV of 300 000 h^{-1}, indicating that this catalyst is effectively resistant against high space velocity.

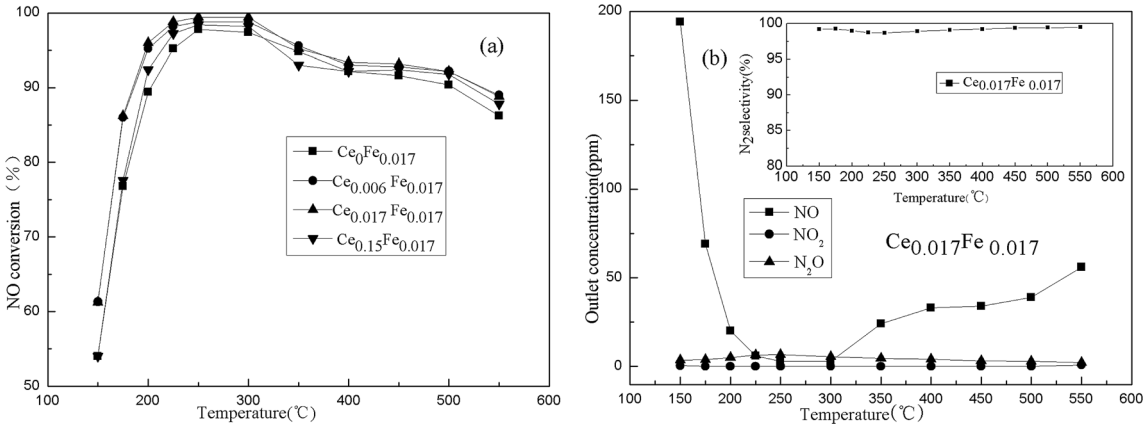

Fig. 1 NO conversion over Ce_x–Fe_y/Cu–SSZ-13 catalysts under GHSV of 150 000 h^{-1} (a), N_2 selectivity of $Ce_{0.017}$–$Fe_{0.017}$/Cu–SSZ-13 catalyst (b).

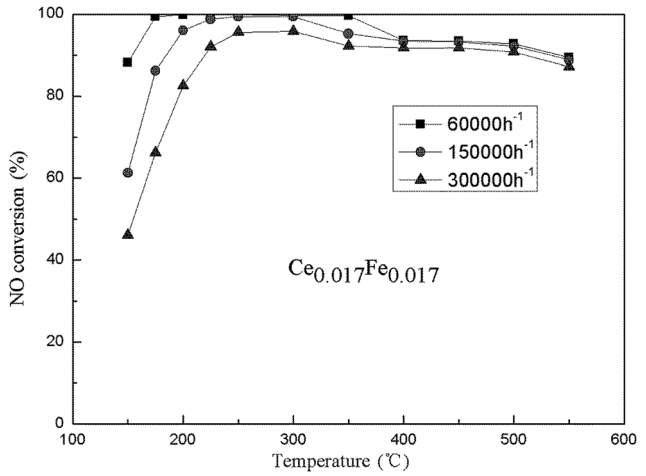

Fig. 2 NH_3–SCR activity over $Ce_{0.017}$–$Fe_{0.017}$/Cu–SSZ-13 under different GHSV.

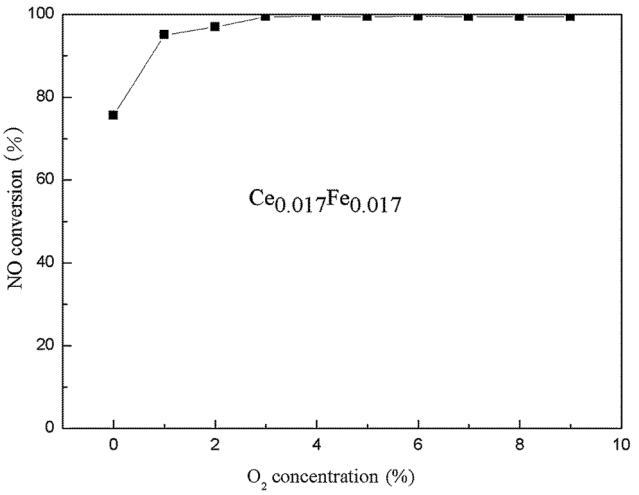

Fig. 3 NH_3–SCR activity over $Ce_{0.017}$–$Fe_{0.017}$/Cu–SSZ-13 catalyst at 300 °C under GHSV of 150 000 h^{-1} at different O_2 concentration.

The effect of O_2 concentration on the SCR activity

The influence of O_2 concentration on NO conversion over $Ce_{0.017}$–$Fe_{0.017}$/Cu–SSZ-13 catalyst was investigated at 300 °C under 150 000 h^{-1} and the result is shown in Fig. 3. The NO conversion increased from 75.6% to 99.4% with the concentration of O_2 increasing from 0 to 3 vol%. The increased catalytic activity might be related to the role that O_2 played in the reaction. Two possible explanations may be that the main role of O_2 is H-abstraction from adsorbed NH_3, resulting in NH_2 species, and secondly, O_2 may be needed to react with NO to form an active intermediate species.[16–18] However, as the concentration of O_2 continued to increase, NO conversion remained unchanged indicating that O_2 is saturated.

The influences of SO_2, CO_2 and H_2O on NH_3–SCR activity

Fig. 4(a) shows the effects of H_2O and SO_2 on the catalytic activity of $Ce_{0.017}$–$Fe_{0.017}$/Cu–SSZ-13 catalyst at 300 °C under 150 000 h^{-1}. When 5 vol% H_2O was added, the activity of the catalyst remained at the previous high level at 300 °C. This suggested that the catalyst was highly water-resistant under these SCR conditions. When 100 ppm SO_2 was added into the feed gases, there was a slight decrease in the NO conversion. The decrease was attributed to the competitive adsorption between SO_2 and NO,[19] so the conversion was restored to its original level after removing SO_2. However, when 100 ppm SO_2 and 5% H_2O were injected into the reaction system simultaneously, NO conversion decreased considerably compared with only 100 ppm SO_2 or 5 vol% H_2O, which might be related to the formation of sulfates that could poison the active sites or block the zeolite pores and the competitive adsorption between SO_2 and NO on the active sites.[20] The effects of H_2O and CO_2 on the catalytic activity of $Ce_{0.017}$–$Fe_{0.017}$/Cu–SSZ-13 catalyst are illustrated in Fig. 4(b). It is clear that pure CO_2 and the co-presence of CO_2 and H_2O in feed gases had almost no effect on NO conversion.

Fig. 5 shows the effect of Ce doping on SO_2 resistance. It is clear that Ce-doped catalyst ($Ce_{0.017}$–$Fe_{0.017}$/Cu–SSZ-13) showed a remarkable enhancement in sulfur–water tolerance compared

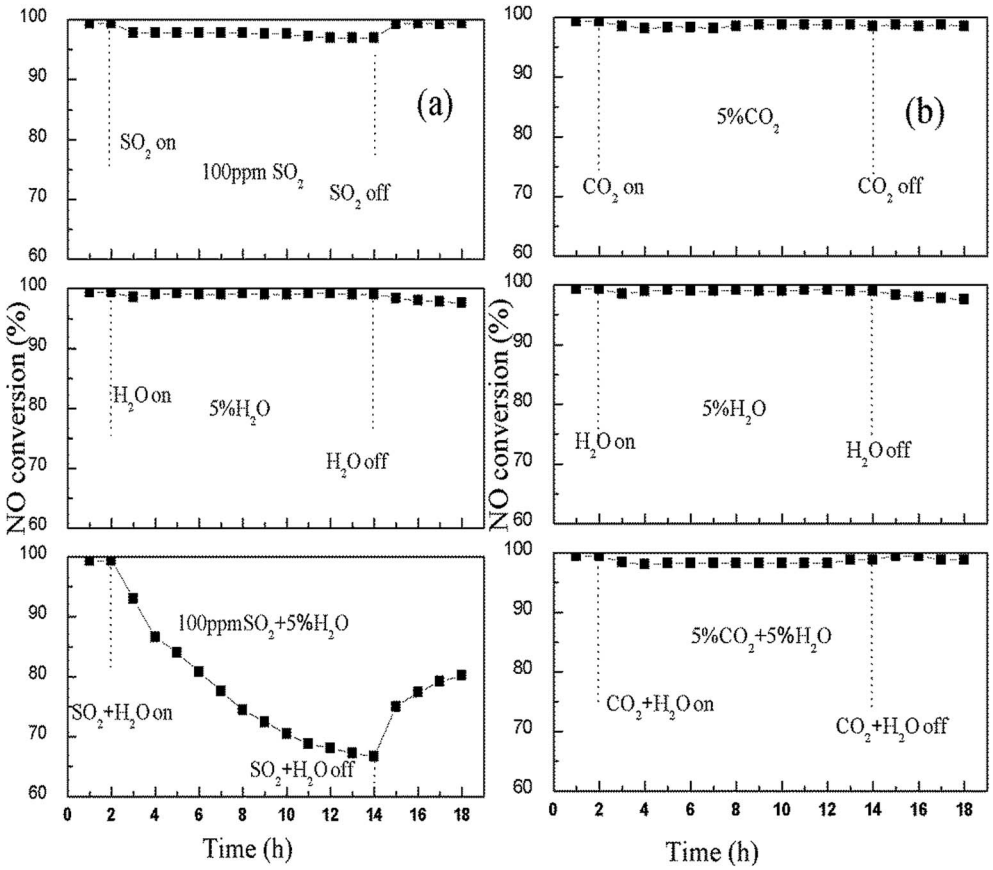

Fig. 4 NO conversion over $Ce_{0.017}$–$Fe_{0.017}$/Cu–SSZ-13 catalyst at 300 °C under GHSV of 150 000 h^{-1} in the co-presence of H_2O + SO_2 (a); H_2O + CO_2 (b).

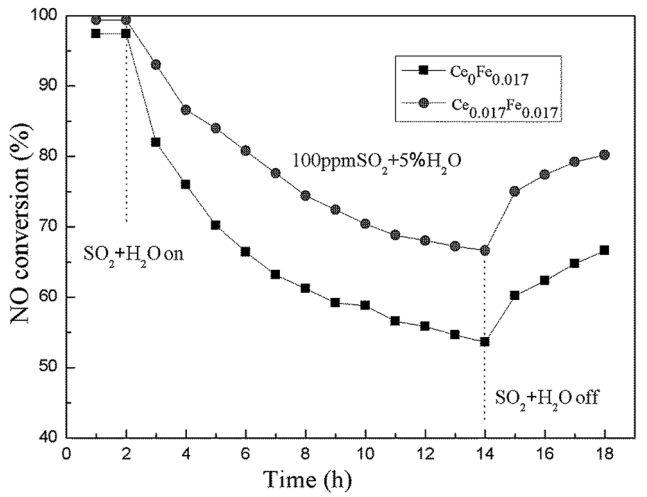

Fig. 5 NO conversion over Ce_0–$Fe_{0.017}$/Cu–SSZ-13 and $Ce_{0.017}$–$Fe_{0.017}$/Cu–SSZ-13 at 300 °C under GHSV of 150 000 h^{-1} in the co-presence of H_2O + SO_2.

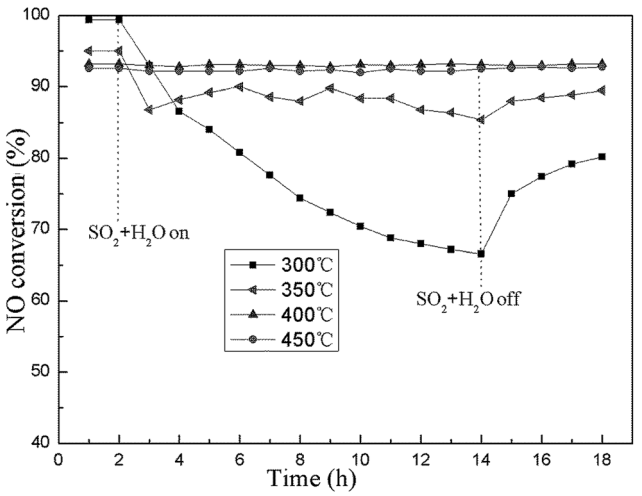

Fig. 6 NO conversion over $Ce_{0.017}$–$Fe_{0.017}$/Cu–SSZ-13 at different temperature under GHSV of 150 000 h^{-1} in the co-presence of H_2O + SO_2.

with Ce_0–$Fe_{0.017}$/Cu–SSZ-13. The improvement of sulfur tolerance might be attributed to the fact that the doping of Ce could efficiently retard the formation of surface sulfation species.[21]

Fig. 6 shows the effect of temperature on SO_2 resistance of $Ce_{0.017}$–$Fe_{0.017}$/Cu–SSZ-13. A continuous decline in NO conversion from 99.4% to 66.6% occurred after 100 ppm SO_2 and 5 vol% H_2O were added for 12 h at 300 °C. When the temperature

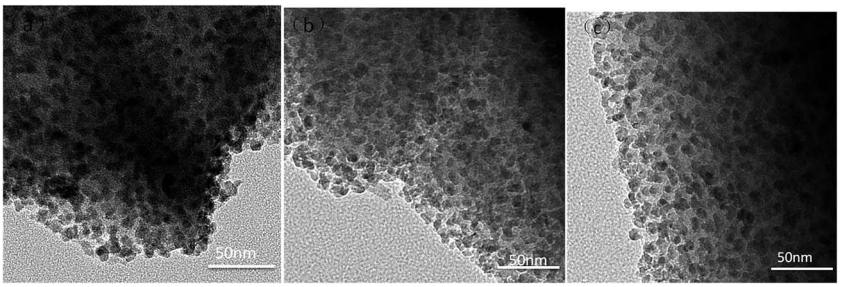

Fig. 7 TEM images of $Ce_{0.006}$–$Fe_{0.017}$/Cu–SSZ-13 (a), $Ce_{0.017}$–$Fe_{0.017}$/Cu–SSZ-13 (b) and $Ce_{0.15}$–$Fe_{0.017}$/Cu–SSZ-13 (c).

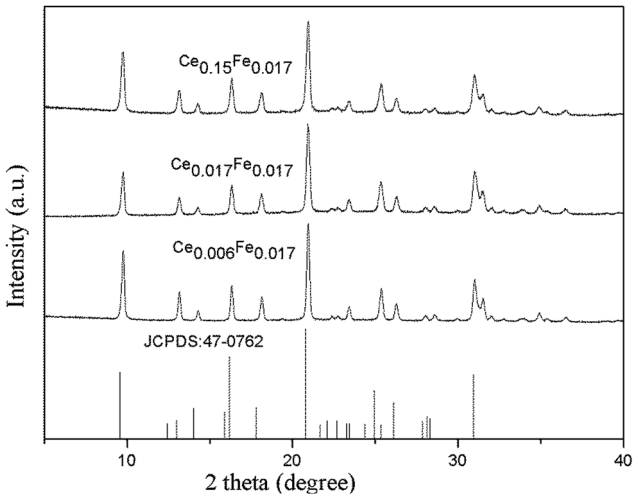

Fig. 8 XRD patterns of Ce_x–Fe_y/Cu–SSZ-13 catalysts and JCPDS reference of SSZ-13 zeolite.

was maintained at 350 °C, NO conversion decreased from 95% to 86.8% after 100 ppm SO_2 and 5 vol% H_2O were added for 1 h, then the NO conversion became stable for another 11 h. The deactivation role of SO_2 over the catalyst might be related to the formation of ammonium sulfate. $(NH_4)_2SO_4$ decomposition involves the initial decomposition to NH_3 and NH_4HSO_4 at around 300 °C and the subsequent decomposition of surface NH_4HSO_4 species to NH_3 and SO_2 at 350 °C.[20,22] After removal of SO_2 and H_2O, NO conversion restored to some extent at both 300 °C and 350 °C. Obviously, there was almost no effect of SO_2 and H_2O on the NO conversion when the temperature is higher than 400 °C. The results above suggested that the impact of SO_2 on NO conversion could be eliminated by increasing the temperature.

The results of TEM

Fig. 7 shows the TEM micrographs of $Ce_{0.006}$–$Fe_{0.017}$/Cu–SSZ-13, $Ce_{0.017}$–$Fe_{0.017}$/Cu–SSZ-13 and $Ce_{0.15}$–$Fe_{0.017}$/Cu–SSZ-13. The small dark spots were attributed to oxide metal nanoparticles (CeO_2, α-Fe_2O_3 and CuO) and the faint background represented the SSZ-13 support. It can be clearly seen that, oxide metal nanoparticles are well dispersed on the surface of the catalysts.

XRD patterns results

The XRD patterns of Ce_x–Fe_y/Cu–SSZ-13 catalysts and JCPDS reference of SSZ-13 are shown in Fig. 8. All catalysts exhibited the characteristic peaks corresponding to SSZ-13 zeolite structure ($2\theta = 9.5°$, 14.0°, 16.1°, 17.8°, 20.7°, 25.0°, 26.1° and 30.9°) with a perfect degree of crystallization, indicating that the original zeolite structure remained intact. The diffraction peaks of CeO_2, α-Fe_2O_3 and CuO were not observed among all

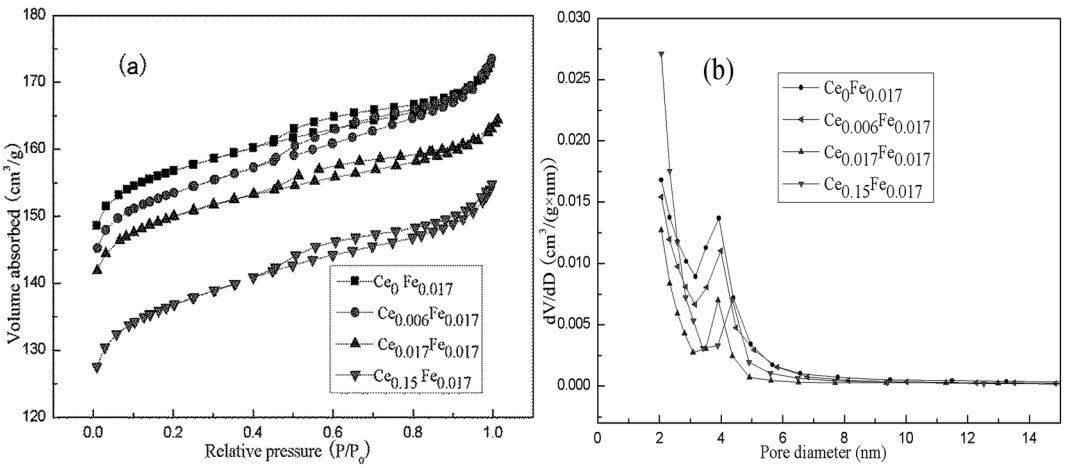

Fig. 9 N_2 adsorption–desorption isotherms (a) and pore-size distribution curves (b) of Ce_x–Fe_y/Cu–SSZ-13 catalysts.

Table 1 The physicochemical properties of Ce_x–Fe_y/Cu–SSZ-13 catalysts

Sample	S_{BET}[a] ($m^2\ g^{-1}$)	Pore volume[b] ($cm^3\ g^{-1}$)	Average pore diameter[c] (nm)	Concentration[d] (wt%)		
				Ce	Fe	Cu
Ce_0–$Fe_{0.017}$/Cu–SSZ-13	522	0.220	3.90	—	3.44	1.27
$Ce_{0.006}$–$Fe_{0.017}$/Cu–SSZ-13	511	0.214	3.97	0.67	3.10	1.11
$Ce_{0.017}$–$Fe_{0.017}$/Cu–SSZ-13	503	0.194	3.91	0.82	3.48	1.14
$Ce_{0.15}$–$Fe_{0.017}$/Cu–SSZ-13	458	0.186	4.31	0.87	3.28	1.10

[a] Calculated by BET method. [b] Calculated by *t*-plot method. [c] Calculated using the BJH method with desorption branch. [d] Characterized by ICP-OES.

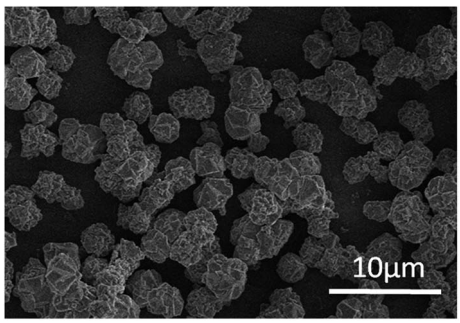

Fig. 10 SEM images of $Ce_{0.017}$–$Fe_{0.017}$/Cu–SSZ-13.

Table 2 Metal dispersion (%) of $Ce_{0.017}$–$Fe_{0.017}$/Cu–SSZ-13

Sample	Metal dispersion[a] (%)		
	Ce	Fe	Cu
$Ce_{0.017}$–$Fe_{0.017}$/Cu–SSZ-13	84.76	100	25.09

[a] Metal dispersion (%) = the number of metal atoms on the surface/total number of metal atoms in the bulk.

catalysts, indicating that the copper, iron and cerium species as oxide metal nanoparticles were well dispersed on the surface of SSZ-13 support, which was confirmed by the results of TEM images.

The results of BET

Fig. 9 shows the results of N_2 adsorption–desorption isotherms and pore-size distribution of Ce_x–Fe_y/Cu–SSZ-13 catalysts. According to the IUPAC classification, all adsorption–desorption isotherm curves of the samples in Fig. 9(a) can be considered as a combination of type I and type IV, indicating the presence of microporous and slit shaped pores. Fig. 9(b) shows that Ce_0–$Fe_{0.017}$/Cu–SSZ-13, $Ce_{0.006}$–$Fe_{0.017}$/Cu–SSZ-13, $Ce_{0.017}$–$Fe_{0.017}$/Cu–SSZ-13 and $Ce_{0.15}$–$Fe_{0.017}$/Cu–SSZ-13 catalysts have only a narrow visible peak at around 3.94 nm, 3.99 nm, 3.92 nm, and 4.38 nm, respectively, indicating that excessive loading of Ce results in larger pore size. The pore structure parameters of all samples are listed in Table 1. It is clear that the surface area and pore volume of Ce_x–Fe_y/Cu–SSZ-13 catalysts decrease with an increase of cerium content indicating that excessive Ce loading results in agglomeration that blocked the "channel" of catalysts. Remarkably, $Ce_{0.006}$–$Fe_{0.017}$/Cu–SSZ-13 and $Ce_{0.017}$–$Fe_{0.017}$/Cu–SSZ-13 catalysts with larger surface area and smaller pore size exhibit higher catalytic activity compared with $Ce_{0.15}$–$Fe_{0.017}$/Cu–SSZ-13 catalyst which can be concluded from Fig. 1 and Table 1. The results are in accordance with the previous report that larger specific surface areas and smaller pore size are in favor of catalytic reaction.[23]

The results of SEM

The SEM micrographs of $Ce_{0.017}$–$Fe_{0.017}$/Cu–SSZ-13 are shown in Fig. 10. It is clear that the sample was made of hexagonal crystals. The average particle size of the catalyst is about 2.5 μm. In addition, It can be seen from the image that the catalyst shows perfect degree of crystallization which is in accordance with the XRD results.

The metal dispersion

The metal dispersion of $Ce_{0.017}$–$Fe_{0.017}$/Cu–SSZ-13 determined by XPS and ICP is shown in Table 2. It is clear that Fe and Ce species are mostly dispersed on the surface of the catalyst $Ce_{0.017}$–$Fe_{0.017}$/Cu–SSZ-13 through post-synthesis cation exchanges. The good metal dispersion is favorable to the synergetic effects.

Conclusions

A series of CHA-type trimetallic composite zeolites of Ce_x–Fe_y/Cu–SSZ-13 catalysts were prepared by the one-pot synthesized Cu–SSZ-13 and subsequent ion-exchange with Fe^{3+} and Ce^{3+}. The XRD results revealed that the zeolite structure remained intact after both Fe and Ce incorporation into Cu–SSZ-13. The SEM micrographs showed that the sample was made of hexagonal crystals. $Ce_{0.017}$–$Fe_{0.017}$/Cu–SSZ-13 have a large BET specific surface area (503 $m^2\ g^{-1}$) and a narrow pore size distribution (3.92 nm). Excessive Ce loading would result in agglomeration that blocked the "channel" of catalysts. Larger specific surface areas and smaller pore size favor a catalytic reaction, which can be concluded from the catalytic performance tests and the results of BET. Among the prepared Ce_x–Fe_y/Cu–SSZ-13 catalysts, $Ce_{0.017}$–$Fe_{0.017}$/Cu–SSZ-13 catalyst showed the best catalytic performance. The good metal dispersion of $Ce_{0.017}$–$Fe_{0.017}$/Cu–SSZ-13 was favorable to the synergetic effects. It presented

super NH_3–SCR activity, excellent N_2 selectivity in a relatively wide temperature range, strong resistance to high space velocity as well as good tolerance to CO_2 and H_2O. In addition, $Ce_{0.017}$–$Fe_{0.017}$/Cu–SSZ-13 (Ce-doped catalyst) showed a remarkable enhancement in sulfur–water tolerance compared with Ce_0–$Fe_{0.017}$/Cu–SSZ-13. The impact of SO_2 on NO conversion could be eliminated by increasing temperature. Further studies on the mechanism of the reaction are in progress.

References

1 P. Granger and V. I. Parvulescu, *Chem. Rev.*, 2011, **111**, 3155–3207.
2 U. Deka, I. Lezcano-Gonzalez, S. J. Warrender, A. L. Picone, P. A. Wright, B. M. Weckhuysen and A. M. Beale, *Microporous Mesoporous Mater.*, 2013, **166**, 144–152.
3 X. F. Yang, Z. L. Wu, M. Moses-Debusk, D. R. Mullins, S. M. Mahurin, R. A. Geiger, M. Kidder and C. K. Narula, *J. Phys. Chem. C*, 2012, **116**, 23322–23331.
4 J. H. Kwak, R. G. Tonkyn, D. H. Kim, J. Szanyi and C. H. F. Peden, *J. Catal.*, 2010, **275**, 187–190.
5 S. J. Schmieg, S. H. Oh, C. H. Kim, D. B. Brown, J. H. Lee, C. H. F. Peden and D. H. Kim, *Catal. Today*, 2012, **184**, 252–261.
6 S. I. Zones, *US Pat.*, 4 544 538, 1985.
7 S. I. Zones, *J. Chem. Soc., Faraday Trans.*, 1991, **87**, 3709–3716.
8 N. Martín, M. Moliner and A. Corma, *Chem. Commun.*, 2015, **51**, 9965–9968.
9 B. H. Chen, R. N. Xu, R. D. Zhang and N. Liu, *Environ. Sci. Technol.*, 2014, **48**, 13909–13916.
10 L. M. Ren, L. F. Zhu, C. G. Yang, Y. M. Chen, Q. Sun, H. Y. Zhang, C. J. Li, F. Nawaz, X. J. Meng and F. S. Xiao, *Chem. Commun.*, 2011, **47**, 9789–9791.
11 L. J. Xie, F. D. Liu, L. M. Ren, X. Y. Shi, F. S. Xiao and H. He, *Environ. Sci. Technol.*, 2014, **48**, 566–572.
12 R. R. Zhang, Y. H. Li and T. L. Zhen, *RSC Adv.*, 2014, **4**, 52130–52139.
13 X. Gao, Y. Jiang, Y. C. Fu, Y. Zhong, Z. Y. Luo and K. Cen, *Catal. Commun.*, 2010, **11**, 465–469.
14 E. Ito, Y. J. Mergler, B. E. Nieuwenhuys, H. V. Bekkum and C. M. V. D. Bleek, *Microporous Mater.*, 1995, **4**, 455–465.
15 T. T. Gu, Y. Liu, X. L. Weng, H. Q. Wang and Z. B. Wu, *Catal. Commun.*, 2010, **12**, 310–313.
16 K. S. Kijlstra, D. S. Brands, H. I. Smit, E. K. Poels and A. Bliek, *J. Catal.*, 1997, **171**, 219–230.
17 K. S. Kijlstra, D. S. Brands, E. K. Poels and A. Bliek, *J. Catal.*, 1997, **171**, 208–218.
18 H. Sjövall, L. Olsson, E. Fridell and R. J. Blint, *Appl. Catal., B*, 2006, **64**, 180–188.
19 Y. T. Li and Q. Zhong, *J. Hazard. Mater.*, 2009, **172**, 635–640.
20 L. Zhang, D. Wang, Y. Liu, K. Kamasamudram, J. H. Li and W. Epling, *Appl. Catal., B*, 2014, **156**, 371–377.
21 R. B. Jin, Y. Liu, Y. Wang, W. L. Cen, Z. B. Wu, H. Q. Wang and X. L. Weng, *Appl. Catal., B*, 2014, **148**, 582–588.
22 I. S. Nam, J. W. Eldridge and J. R. Kittrell, *Ind. Eng. Chem. Prod. Res. Dev.*, 1986, **25**, 192–197.
23 J. H. Park, H. J. Park, J. H. Baik, I. S. Nam, C. H. Shin, J. H. Lee, B. K. Cho and S. H. Oh, *J. Catal.*, 2006, **240**, 47–57.